Towards a bio-inspired acoustic sensor: *Achroia grisella*'s ear

Lara Díaz-García*, *Student Member, IEEE*, Andrew Reid, Joseph Jackson, James F.C. Windmill, *Senior Member, IEEE*
Centre for Ultrasonic Engineering, University of Strathclyde, Glasgow, United Kingdom
* Corresponding author: lara.diaz-garcia@strath.ac.uk

***Abstract*— Bio-inspiration looks to nature to overcome challenges innovatively. Insects show many examples of efficient approaches to hearing considering the small sizes of their bodies. The nocturnal moth *Achroia grisella* is capable of directional hearing of wavelengths several times larger than the separation between its tympana. Directionality in this moth seems to be monoaural and dependent exclusively on morphology, so a model is developed to replicate the structure. We start from a simple circular model, progressively incorporating more complex elements to improve the resemblance to the natural system. The goal is to develop a model inspired by *Achroia*'s ear, that behaves similarly to it, and to 3D print devices that agree with the model. Equations, simulations, and 3D printed devices measured through Laser Doppler Vibrometry are compared.**

Keywords*— bio-inspiration; Achroia grisella; insect hearing; 3D printing; acoustic sensor

I. Introduction

Hearing is an important ability through which many animals interact with their environments. Localizing the stimuli source is key for tasks such as avoiding predators, locating preys, or finding a mating partner, some of the principal purposes for which hearing is used. Directional hearing is, therefore, a desirable trait. All animals that hear (except for mantids) present bilateral symmetry in their bodies, which means most of them have one ear (in the broader sense of the word) in each half of their bodies. Bigger animals can achieve directional hearing by comparing intensity, phase, or time of arrival between their two ears, but smaller animals, for which the inter-ear distance is too small for any of these differences to be meaningful, must resort to alternative, inventive methods to locate the origin of sounds [1].

Insects' bodies sizes are generally small. Not all of them possess a hearing sense that we know about, but some have found a way around the size limitation to hear frequencies with wavelengths of the same scale as their bodies. Some have different openings in their tracheal system to the outside in order to allow soundwaves to arrive to the outside and inside of their tympana, like grasshoppers [2] or field crickets [3]. Others, like the well-studied *Ormia ochracea*, have a stiff tissue bridge between their two tympana, making the whole system behave in a complex way with different resonances that allows them to land on their host with a 2º precision, even when the frequency of the host call is considerably larger than the fly's size [4]–[7].

Achroia grisella is a pyraloid moth that is uncommon in that its mating process involves the male calling the female through ultrasonic signals. Even though hearing is widespread in the *Pyraloidea* superfamily, interspecific acoustic communication is uncommon [8]. Their rudimentary hearing system is believed to have evolved to avoid their main predator, the bat, and later repurposed [9]. *Achroia*, when exposed to a bat's echolocation call, drops towards the ground if flying or stops moving completely if walking. On the other hand, during the mating process, male specimens produce a series of ultrasound pairs of pulses (main content of the signal of 100 kilohertz [10]) that the females orientate towards not optimally but efficiently enough to guarantee mating. The moths have only 3 neurons per tympanum, and they have been proven unable to discriminate frequencies. The threshold of the stimulus signal for different behavior (evasive or positive) in the moth is thus believed to be time-encoded [11]. *Achroia grisella*'s average size means that their tympana are separated less than 600 microns. This distance is insufficient to account for any phase, intensity, or time of arrival difference between their ears considering a 100 kilohertz signal has a wavelength of 3.8 millimeters. On the other hand, no connection has been detected between the tympana using X-ray scanning, no spiracles are found either [12], and the measurements of diffraction in the abdominal section of the moth do not provide enough intensity difference [13]. Furthermore, moths with one tympanum pierced and the other one in healthy condition were still able to locate the singing males, if only taking a longer time [14]. It is therefore believed that the directionality must be achieved monoaurally and purely through the geometry of the tympana themselves.

II. Analytical and Simulation Approach

Our working hypothesis is that the *Achroia grisella*'s tympanum must confer them with some degree of directionality. We start by posing a simple model and progressively increasing its complexity by adding new elements to it. The problem is considered through Finite Element Modelling (FEM) using COMSOL Multiphysics® and analytically.

Achroia grisella's tympana are roughly elliptic in shape, divided in two sections of different thicknesses (the thicker one called *conjunctivum* and the thinner one called tympanic membrane or *tympanum proper*), and have the *scolopidium*, a cluster of three periphery neurons, directly attached somewhere close to the center of the thinner region (Fig. 1). Through Laser Doppler Vibrometry, an *Achroia* tympanum is observed when exposed to a signal of 100 kilohertz. The displacement pattern of the membrane is complex and not drum-like. A large peak dominates the displacement close to the neuron attachment point; a series of secondary peaks

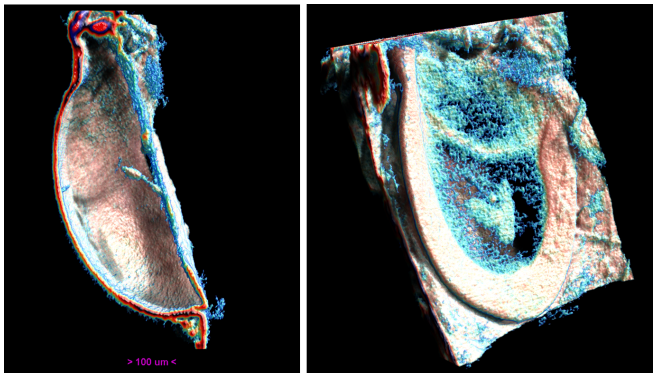

Fig. 1. Voxel reconstruction of Achroia grisella tympanum from X-ray microtomography. (Left) Side view cross section along major axis showing tympanal cavity and scolopidium. (Right) Tympanum face showing attachment point and ridge connecting upper and lower membranes.

appear in a ring formation around the main peak; and a very broad, low amplitude bump is seen in the *conjunctivum* [15].

To obtain an analytical solution, we consider the equation for transverse vibrations on a plate:

$$\nabla^2(\nabla^2 W) + \frac{1}{c^2} \cdot \frac{\delta^2 W}{\delta t^2} = 0 \qquad (1)$$

Where $\nabla^2\nabla^2 = \nabla^4$ is known as the biharmonic operator, $W = W(x, y, t)$ and describes displacement, and c is the velocity of the wave in the medium and is defined as:

$$c = \sqrt{\frac{E \cdot h^2}{12 \cdot \rho \cdot (1 - \nu^2)}} \qquad (2)$$

The parameters being Young's modulus (E), thickness (h), mass volume density (ρ), and Poisson's ratio (ν). The resolution of equation (1) gives us the eigenvalues for the problem which in turn are related to the natural frequencies of vibration of the plates. The reason we consider plates and not membranes is because stiffness is not negligible.

By assuming a periodical dependence on time, we can simplify the equation and solve for the specific boundary conditions of our problem. We consider plates clamped all around, such as is the case of the moth's tympana. The sizes considered both for the equations and simulations are approximated from measurements on actual specimens of *Achroia grisella* [15]. The values for Young's modulus, mass volume density, and Poisson's ratio are taken to be 1 gigapascal, 1180 kilograms per cubic meter and 0.35, all within the range of values for insect cuticle. Young's modulus is chosen in the lower end of the range of values for sclerotized cuticle. [16]

A. Circular plate

The first model is a circular plate in vacuum. This model is easily solved and simulated, and the first six eigenfrequencies and their corresponding mode shapes are obtained. The circular plate considered is 500 microns in diameter and 5 microns in thickness. We use polar coordinates, and the resolution involves Bessel functions. There is a good agreement between COMSOL and predicted eigenfrequencies, with differences below 1%.

B. Elliptical plate

The next step is considering an elliptical solid plate, which complicates the analytical solution significantly because elliptical coordinates and Mathieu functions need to be used [17], [18]. The elliptical plate has major and minor axes of 670 and 500 microns respectively, and a thickness of 5 microns. The resonance frequencies in the elliptical plates are related to the eigenvalues obtained from the application of the clamped boundary conditions at the perimeter of the ellipse:

$$f_{m,n} = \frac{2 \cdot q_{m,n} \cdot c}{\pi \cdot (a^2 - b^2)}, m = 0,1,2 \ldots, n = 1,2,3 \ldots \qquad (3)$$

Where the resonance frequencies ($f_{m,n}$) depend on the eigenvalues ($q_{m,n}$), the velocity of the wave in the medium (c) and the major and minor semi-axes of the ellipse (a and b respectively). There is also good agreement between COMSOL and predicted eigenfrequencies, with differences below 7%. The patterns of vibration of this and the previous model are still far from resembling the moth tympanum's movement.

C. Elliptical plate: double thickness and point mass

The next step is considering an elliptical plate divided in two different sections with thicknesses matching those of the thin and thick regions, and an attached point mass on the thinner region, to emulate the neuron attachment. The mass is estimated to be that of the whole plate concentrated on one point. At this point, with the increasing complexity of the model, analytical equations are no longer useful, but the good agreement in the previous two steps between analytical and simulation models is a reassurance that the COMSOL predicted eigenfrequencies are reliable. The division between regions in the model is 350 microns along the major axis for the thinner region and 320 microns for the thicker one, and the attachment point is located at the center of the thin region (175 microns from the center of the major axis of the ellipse). The thicknesses are 3 and 8 microns respectively.

The vibration pattern of this model has visibly changed and is more complex. The sixth mode shape (see Fig. 2) is a very good match for that described in *Achroia grisella*'s tympana [15]. The frequency response of the plate is extracted from a frequency analysis of the system on COMSOL and can be seen in Fig. 3.

III. Methods

3D printing is carried out using an Original Prusa SL1 3D printer and a commercial resin. This printer employs stereolithography technology, and the resin used is Prusa's own Orange Tough, modelled after Acrylonitrile-butadiene-styrene. The thickness of the printed layers in stereolithography depends on exposure time to UV light [19].

The physical properties of the resin are taken as a Poisson's ratio of 0.35 and volumetric mass density of 1180 kilograms per cubic meter [20]. Young's modulus is measured by printing a cantilevered beam of known dimensions and observing its frequency response. Considering beam theory [21], Young's modulus for the material can be extracted from:

$$E = \frac{48 \cdot \pi^2 \cdot \rho \cdot f_n^2 \cdot L^4}{\lambda_n^4 \cdot h^2}, n = 1,2,3 \ldots \qquad (4)$$

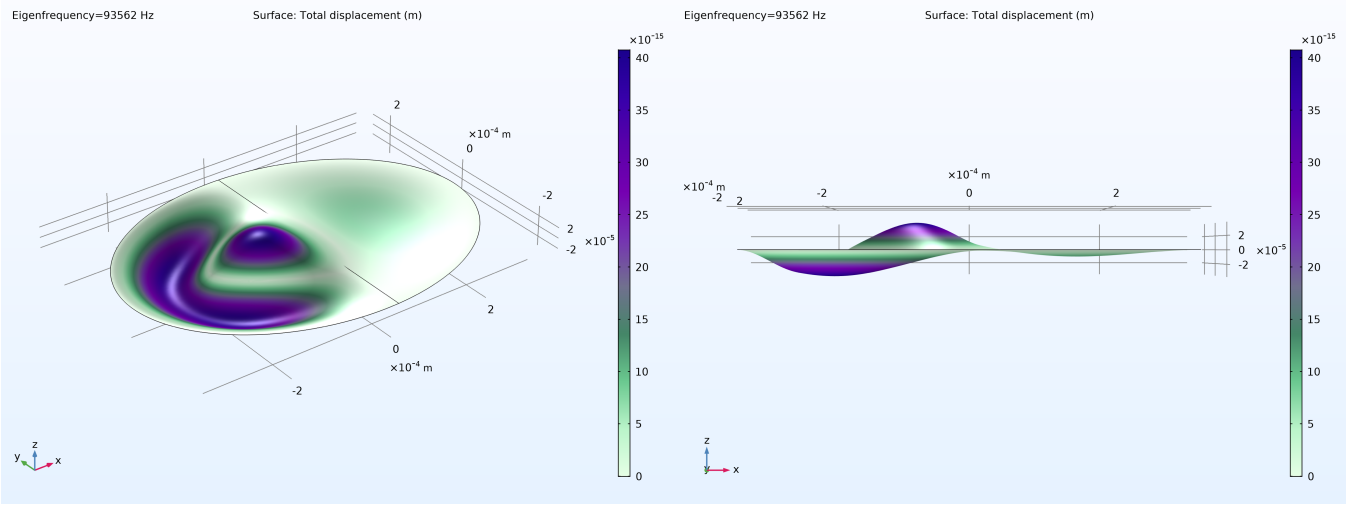

Fig. 2. COMSOL simulation of the sixth natural frequency of an elliptical plate divided in two sections of different thicknesses (thin one on the left half of the ellipse and thick one on the right) with an attached mass (perspective view on the left and XZ plane view on the right).

Where the parameters are Young's modulus (E), mass volume density (ρ), the eigenfrequencies (f_n), the length of the beam (L), the eigenvalues (λ_n) and the thickness (h), all of them known. The value experimentally estimated for Young's modulus is 1.327 gigapascals. The printing size is larger than that of the moth's tympanum. The plates produced have a diameter of 1.5 millimeters for the circular one and major and minor axes of 2.1 and 1.5 millimeters respectively for the elliptical ones. The thickness was measured through X-ray Computer Tomography using a Bruker Skyscan 1172 with SHT 11-megapixel camera and Mamamatsu 80 kilovolts (100 milliamps) source and found to be 162 microns for single layers and 270 microns for the thicker multi-layer regions. It is worth mentioning that 3D printing of small devices is complicated, with residual stress gradients severely affecting the result [22]–[25]. Repeatability and accuracy can be difficult to achieve.

The printed devices are examined in a 3D laser Doppler vibrometer (3D LDV) system with an MSA-100-3D scanning head (Polytec, Waldbrom, Germany). The devices are stimulated with a displacement piezo chip (75 volts, 2.8 microns, Thorlabs, Newton, New Jersey), with wideband periodic burst signals, and their frequency response is recorded. The resonances are found in the LDV scan and compared against the COMSOL simulation eigenfrequencies, re-run with parameters that match those of the 3D printed devices.

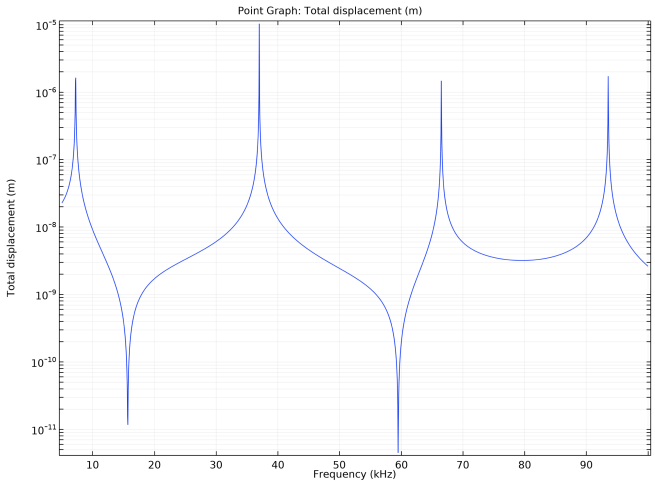

Fig. 3: Frequency response of the elliptical plate with two sections of different thicknesses and a point mass attached.

In Table 1, we can see a side-by-side comparison of the predicted eigenfrequencies and the actual eigenfrequencies of the printed plates. They are in good agreement and mode shapes are recognizable in the LDV scans. The 3D printing is successful, and the devices' behavior matches that predicted by simulation.

IV. Conclusions

Our aim was to develop a model that emulates the behavior of *Achroia grisella*'s tympanum. As we saw in Fig. 2, this objective was achieved satisfactorily. The secondary goal was to 3D print parts that agree with the models; parts were fruitfully produced, which is discussed in Table 1. Further work will delve into studying the directionality of the model in simulations and the directionality of 3D printed parts with experimental techniques.

TABLE I. Comparison between experimental 3D printed plates and COMSOL simulated plates.

	Resonance	COMSOL frequency	Experimental frequency
Circular	1st	135 kHz	137 kHz
	2nd	257 kHz	260 kHz
	3rd	257 kHz	260 kHz
Elliptical	1st	106 kHz	93 kHz
	2nd	174 kHz	167 kHz
	3rd	228 kHz	230 kHz
	4th	262 kHz	258 kHz
Elliptical (Two thicknesses)	1st	129 kHz	127 kHz
	2nd	209 kHz	202 kHz
	3rd	266 kHz	260 kHz
	4th	302 kHz	305 kHz

REFERENCES

[1] D. Robert, 'Directional Hearing in Insects', in *Sound Source Localization*, A. N. Popper and R. R. Fay, Eds. New York, NY: Springer, 2005, pp. 6–35, doi: https://doi.org/10.1007/0-387-28863-5_2

[2] J. Schul, M. Holderied, D. Von Helversen, and O. Von Helversen, 'Directional hearing in grasshoppers: neurophysiological testing of a bioacoustic model', *J. Exp. Biol.*, vol. 202, no. 2, p. 121, 1999.

[3] A. Michelsen, A. V. Popov, and B. Lewis, 'Physics of directional hearing in the cricket Gryllus bimaculatus', *J. Comp. Physiol. A*, vol. 175, no. 2, pp. 153–164, Aug. 1994, doi: 10.1007/BF00215111.

[4] R. S. Edgecomb, D. Robert, M. P. Read, and R. R. Hoy, 'The tympanal hearing organ of a fly: phylogenetic analysis of its morphological origins', *Cell Tissue Res.*, vol. 282, no. 2, pp. 251–268, Nov. 1995, doi: 10.1007/BF00319116.

[5] R. N. Miles, D. Robert, and R. R. Hoy, 'Mechanically coupled ears for directional hearing in the parasitoid fly Ormia ochracea', *J. Acoust. Soc. Am.*, vol. 98, no. 6, p. 3059, Jun. 1998, doi: 10.1121/1.413830.

[6] A. C. Mason, M. L. Oshinsky, and R. R. Hoy, 'Hyperacute directional hearing in a microscale auditory system', *Nature*, vol. 410, no. 6829, pp. 686–691, Apr. 2001, doi: 10.1038/35070564.

[7] W. H. Cade, M. Ciceran, and A.-M. Murray, 'Temporal patterns of parasitoid fly (Ormia ochracea) attraction to field cricket song (Gryllus integer)', *Can. J. Zool.*, Feb. 2011, doi: 10.1139/z96-046.

[8] M. D. Greenfield, 'Acoustic Communication in the Nocturnal Lepidoptera', in *Insect Hearing and Acoustic Communication*, B. Hedwig, Ed. Berlin, Heidelberg: Springer, 2014, pp. 81–100, doi: https://doi.org/10.1007/978-3-642-40462-7_6

[9] G. S. Pollack, A. C. Mason, A. N. Popper, and R. R. Fay, *Insect hearing*. Springer, 2016.

[10] L. Knopek and C. Hintze-Podufal, 'Uber den Bau der abdominalen Tympanalorgane der Kleinen Wachsmotte Achroia grisella (Fbr.)', *Zool. Jahrbuecher Abt. Fuer Anat. Ontog. Tiere*, vol. 1141, pp. 83–93, Jan. 1986.

[11] R. L. Rodríguez and M. D. Greenfield, 'Behavioural context regulates dual function of ultrasonic hearing in lesser waxmoths: bat avoidance and pair formation', *Physiol. Entomol.*, vol. 29, no. 2, pp. 159–168, 2004, doi: https://doi.org/10.1111/j.1365-3032.2004.00380.x.

[12] J. L. Eaton, *Lepidopteran anatomy*. New York; Chichester; Brisbane: J. Wiley & Sons, 1988.

[13] A. Reid, T. Marin-Cudraz, J. F. Windmill, and M. D. Greenfield, 'Evolution of directional hearing in moths via conversion of bat detection devices to asymmetric pressure gradient receivers', *Proc. Natl. Acad. Sci.*, vol. 113, no. 48, pp. E7740–E7748, 2016.

[14] H. G. Spangler and C. L. Hippenmeyer, 'Binaural phonotaxis in the lesser wax moth,Achroia grisella (F.) (Lepidoptera: Pyralidae)', *J. Insect Behav.*, vol. 1, no. 1, pp. 117–122, Jan. 1988, doi: 10.1007/BF01052508.

[15] A. Reid, 'Directional hearing at the micro-scale: bio-inspired sound localization', University of Strathclyde, 2017.

[16] J. F. V. Vincent and U. G. K. Wegst, 'Design and mechanical properties of insect cuticle', *Arthropod Struct. Dev.*, vol. 33, no. 3, pp. 187–199, Jul. 2004, doi: 10.1016/j.asd.2004.05.006.

[17] A. W. Leissa, *Vibration of Plates*. Scientific and Technical Information Division, National Aeronautics and Space Administration, 1969.

[18] J. C. Gutiérrez-Vega, R. M. Rodríguez-Dagnino, M. A. Meneses-Nava, and S. Chávez-Cerda, 'Mathieu functions, a visual approach', *Am. J. Phys.*, vol. 71, no. 3, pp. 233–242, Feb. 2003, doi: 10.1119/1.1522698.

[19] H. Gong, M. Beauchamp, S. Perry, A. T. Woolley, and G. P. Nordin, 'Optical approach to resin formulation for 3D printed microfluidics', *RSC Adv.*, vol. 5, no. 129, pp. 106621–106632, 2015.

[20] H. Mao *et al.*, 'Twist, tilt and stretch: From isometric Kelvin cells to anisotropic cellular materials', *Mater. Des.*, vol. 193, p. 108855, Aug. 2020, doi: 10.1016/j.matdes.2020.108855.

[21] J. M. Gere and S. P. Timoshenko, *Mechanics of materials*. Boston: PWS Publishing Company, 1997.

[22] D. Wu, Z. Zhao, Q. Zhang, H. Jerry Qi, and D. Fang, 'Mechanics of shape distortion of DLP 3D printed structures during UV post-curing', *Soft Matter*, vol. 15, no. 30, pp. 6151–6159, 2019, doi: 10.1039/C9SM00725C.

[23] J. Wu *et al.*, 'Evolution of material properties during free radical photopolymerization', *J. Mech. Phys. Solids*, vol. 112, pp. 25–49, Mar. 2018, doi: 10.1016/j.jmps.2017.11.018.

[24] P. S. Bychkov, V. M. Kozintsev, A. V. Manzhirov, and A. L. Popov, 'Determination of Residual Stresses in Products in Additive Production by the Layer-by-Layer Photopolymerization Method', *Mech. Solids*, vol. 52, no. 5, pp. 524–529, Sep. 2017, doi: 10.3103/S0025654417050077.

[25] A. Reid, J. C. Jackson, and J. F. C. Windmill, 'Voxel based method for predictive modelling of solidification and stress in digital light processing based additive manufacture', *Soft Matter*, vol. 17, no. 7, pp. 1881–1887, Feb. 2021, doi: 10.1039/D0SM01968B.